JOURNAL OF GEOPHYSICAL RESEARCH, VOL. 105, NO. D6, PAGES 7257–7273, MARCH 27, 2000

A Global Morphology of Gravity Wave Activity in the Stratosphere Revealed by the GPS Occultation Data (GPS/MET)

Toshitaka Tsuda and Masahiro Nishida
Radio Atmospheric Science Center, Kyoto University, Kyoto, Japan

Christian Rocken and Randolph H. Ware
GPS/MET Project, GPS Science and Technology (GST) Program
University Corporation for Atmospheric Research (UCAR), Boulder, Colorado

Abstract. Using temperature profiles obtained by the GPS/MET (GPS Meteorology) experiment from April 1995 to February 1997, we have extracted mesoscale temperature perturbations with vertical wavelengths ranging from 2 to 10 km and background Brunt-Väisälä frequency squared, N^2. For each occultation event, we can evaluate a potential energy E_p which is assumed to be caused by atmospheric gravity waves. The monthly mean values of E_p at 15–20 km around Japan showed an annual variation with an enhancement in winter, which is consistent with the climatological behavior of the kinetic energy of gravity waves observed with the MU (middle and upper atmosphere) radar (34.9°N, 136.0°E) from 1985 to 1989. We have then derived the global distribution of E_p at 20–30 km during Northern Hemisphere winter (from November to February). Our analysis shows that the largest E_p values are generally centered around the equator between 25°N and 25°S with considerable longitude variations. Longitudinal variations of E_p at 20–30 km in a latitude range of 30°–60°N are also analyzed, resulting in larger E_p values over the continents than over the Pacific Ocean. Using GPS/MET data without antispoofing, latitudinal variations of E_p are determined in 15–45 km. Although large E_p values are concentrated near the equator at 20–30 km, E_p tends to become larger at midlatitudes at 30–40 km and higher-altitude regions. At midlatitudes, E_p is found to be larger in winter months in both hemispheres. Height variations of E_p indicate a decrease at 25–30 km and a monotonic increase above 30 km.

1. Introduction

Mesoscale wind velocity and temperature fluctuations in the stratosphere are mainly caused by atmospheric gravity waves with vertical scales ranging from a few hundred meters to several kilometers and the wave periods between the Brunt-Väisälä period (about 5 min in the stratosphere) and the inertial period. The dynamical stress due to the breaking of upward propagating gravity waves has been found to be an important momentum source for determining the background wind field. Therefore it is now well appreciated that gravity waves play a crucial role in driving the general circulation of the middle atmosphere. Inclusion of gravity wave effects, by employing various parameterizations, has become necessary for an accurate general circulation model (GCM).

Paper number 1999JD901005.
0148-0227/00/1999JD901005$09.00

A number of mechanisms can excite gravity waves, which have been studied by using a wide variety of observational techniques, measuring the behavior of mesoscale fluctuations in the temperature and wind velocity in the troposphere and middle atmosphere. Interaction of surface winds with topography can become a significant source of gravity waves [e.g., *Sato*, 1990; *Nastrom and Fritts*, 1992]. Mesosphere-stratosphere-troposphere (MST) radar observations at midlatitudes have revealed the annual variation of gravity wave energy associated with jet stream activity [*Murayama et al.*, 1994]. Synoptic-scale meteorological disturbances also excite gravity waves [e.g., *Fritts and Nastrom*, 1992].

In the tropics it is generally thought that gravity waves are mostly generated by cumulus convection. Aircraft observations in the tropical stratosphere have revealed the generation of small-scale disturbances associated with cumulus convection [*Pfister et al.*, 1986, 1993], whose fundamental behavior was compared well qualitatively with a theoretical model of gravity waves [*Alexander and Pfister*, 1995]. *Alexander and Holton*

[1997] further studied the detailed behavior of gravity waves generated by tropical convection using a high-resolution numerical model and described the momentum flux deposition caused by wave damping.

The seasonal and geographical variability of stratospheric gravity waves was studied using a global dataset of meteorological rocket soundings [*Hirota*, 1984; *Hirota and Niki*, 1985; *Hamilton*, 1991]. The analysis was further expanded for long-term rocket data to describe the global morphology of gravity waves [*Eckermann et al.*, 1994]. High-resolution temperature soundings with routine radiosondes over Australia and Antarctica (12°–68°S) were used to determine the distribution of potential energy as a function of season and latitude [*Allen and Vincent*, 1995]. The gravity wave activity in the lower stratosphere (17–24 km) showed an annual variation with a maximum during the rainy season (December–January) in the low latitudes and during winter months (June–August) in the southern midlatitudes.

New satellite-borne remote sensing measurements provide excellent global information on the background dynamical structure, planetary-scale fluctuations, and even mesoscale disturbances [*Fetzer and Gille*, 1994; *Wu and Waters*, 1996a, b; *Preusse et al.*, 1998]. In particular, from high-resolution radiance measurements with the Microwave Limb Sounder (MLS) onboard the Upper Atmosphere Research Satellite (UARS), *Wu and Waters* [1996a, b] extracted temperature fluctuations with horizontal scales less than 100 km and studied a global distribution of gravity wave activity in the stratosphere and mesosphere (30–80 km). At 30–50 km altitudes the variance was enhanced in a high-latitude region during winter. However, above about 60 km, a large variance was detected at middle and high latitudes during summer, which was interpreted as the result of a selective filtering of upward propagating gravity waves affected by the jet stream in the stratosphere. *Alexander* [1998] described the UARS-MLS results with a numerical model, assuming a globally uniform excitation of gravity waves in the troposphere, and concluded that the fundamental patterns of the wave energy at middle and high latitudes do not depend on source distribution. Instead, the latitude distribution of wave energy is chiefly determined by interactions of propagating gravity waves with the background wind, and it is also affected by the atmospheric stability conditions [*Alexander*, 1998].

Because of these intensive observational and theoretical studies, our knowledge of the behavior of gravity waves has greatly advanced in the last decades. Yet the global distribution of gravity wave activity is not known; its better definition is needed to fully understand the wave effects under different geographic and seasonal conditions. This is particularly true in the equatorial stratosphere.

The Global Positioning System/Meteorology (GPS/MET) experiment has recently been initiated by the University Corporation for Atmospheric Research (UCAR), successfully providing the international scientific community with a new global high-resolution data set of temperature, pressure, and refractivity profiles in the 1–60 km height range. These profiles are obtained from the active limb-sounding occultation technique as described by *Ware et al.* [1996] and *Rocken et al.* [1997]. In this experiment a GPS receiver aboard Microlab 1 was launched on April 3, 1995, into a low Earth orbit (LEO) to observe occulted radio signals from the GPS satellites. Height profiles of atmospheric refractive index were derived from these observations. By assuming the hydrostatic relation for a dry atmosphere, temperature profiles can further be inferred. *Rocken et al.* [1997] showed a 1°C mean temperature agreement with the best correlative data between 5 and 40 km.

In this study we have extracted mesoscale temperature perturbations with a vertical scale ranging from 2 to 10 km, as well as the background Brunt-Väisälä frequency squared N^2, from all published GPS/MET temperature profiles between April 1995 and February 1997. We then determined the potential energy E_p, from the temperature variance caused by small vertical scale perturbations as a function of latitude, longitude, season, and altitude, yielding the energy distribution of gravity waves in the stratosphere.

In the following sections we first introduce a spectral model of gravity waves, and, subsequently we describe the data analysis procedure for extracting E_p from GPS/MET temperature profiles. The analyzed results are compared with the climatological behavior of gravity waves observed with the MU (middle and upper atmosphere) radar in Shigaraki, Japan. Finally, we use GPS/MET data to determine the global distribution of E_p caused by gravity waves.

2. Theoretical Consideration of Gravity Wave Energy

Mesoscale fluctuations of the wind velocity and temperature appear as superpositions of many gravity waves with different temporal and spatial scales. Therefore the behavior of gravity waves are often better interpreted in terms of a spectrum as a function of wave frequency ω, and vertical and horizontal wavenumbers m and k. *VanZandt* [1982] investigated observed gravity wave spectra in the troposphere and middle atmosphere and found a universality of the spectra regardless of season, altitude, and geographic conditions. In particular, the frequency and horizontal wavenumber spectra vary approximately as $\omega^{-5/3}$ and $k^{-5/3}$, respectively. Assuming gravity wave saturation due to convective or shear instabilities, *Smith et al.* [1987] further developed a model for the vertical wavenumber spectrum of horizontal wind velocity and temperature, with the logarithmic spectral slope of -3 for large m.

For a profile observed with, for example, MST radar or radiosondes, *Fritts and VanZandt* [1993] described the energy spectrum of wind velocity and temperature perturbations caused by gravity waves, as a product of separable functions in ω, m, and ϕ,

$$E(\mu, \omega, \phi) = E_0 A(\mu) B(\omega) \Phi(\phi), \qquad (1)$$

where

$$A(\mu) = \frac{A_0 \mu^s}{(1+\mu^{s+t})}, \quad (2)$$

$$B(\omega) = B_0 \omega^{-p}. \quad (3)$$

Here $\mu = m/m_*$, $m = 2\pi/\lambda_z$ with λ_z and m_* being the vertical wavelength and the characteristic wavenumber, respectively, and ϕ is the azimuth angle, indicating the direction of wave propagation. The parameters E_0 and A_0 and B_0 are, respectively, the total gravity wave energy per unit mass and normalization constraints for vertical wavenumber and frequency spectra $A(\mu)$ and $B(\omega)$. The function $\Phi(\phi)$ depicts the anisotropy of the wave field.

By fitting to the observed logarithmic slope of spectra, the constants s, t, and p are determined. MST radar observations determined that p is approximately 5/3 to 2.0 [e.g., *Fritts et al.*, 1990]. In later sections we investigate an application of the model spectrum, substituting s=1 and t= 3, respectively. Then, the vertical wavenumber spectrum becomes [*Desaubies*, 1976]

$$A(\mu) = \frac{C\mu}{1+\mu^4}, \quad (4)$$

where C is a constant. From coordinated radar and rocketsonde observations the dominant vertical scale of gravity waves, which is slightly larger than $1/m_*$, was found to increase with altitude, ~2–3 km in the lower stratosphere, ~5–10 km in the upper stratosphere, and longer than 10 km in the mesosphere [*Tsuda et al.*, 1994].

A quantity E_0 is chosen in this study as the measure for gravity wave activity, defined as

$$E_0 = \frac{1}{2}[\overline{u'^2} + \overline{v'^2} + \overline{w'^2} + (\frac{g}{N})^2 \overline{(\frac{T'}{\overline{T}})^2}] = E_k + E_p, \quad (5)$$

where E_k and E_p are kinetic energy and potential energy per unit mass, respectively, given by

$$E_k = \frac{1}{2}[\overline{u'^2} + \overline{v'^2} + \overline{w'^2}], \quad (6)$$

$$E_p = \frac{1}{2}(\frac{g}{N})^2 \overline{(\frac{T'}{\overline{T}})^2}. \quad (7)$$

Here u' and v' correspond to the perturbation components of wind velocity, which are aligned or orthogonal to the wave propagation direction, respectively, while, w' is the vertical wind velocity. However, assuming a uniform azimuthal distribution of wave propagation, we may use the perturbations of the zonal and meridional wind components for u' and v', respectively. $\overline{T}$ and T' are the mean and perturbation components of temperature, and g is the gravitational acceleration.

Accurate measurements of three perturbation components of wind velocity are required to completely define E_k. However, w' is much smaller than the horizontal components, and therefore it can be neglected in E_k. It is noteworthy that u', v', w', and T' are all coupled to each other through the gravity wave polarization equations. A linear theory of gravity waves predicts that the ratio of the kinetic to potential energy, E_k/E_p, is a constant [e.g., *VanZandt*, 1985], equal to the spectral index p (see equation (3)). Therefore under the linear theory it is possible to estimate E_0 from temperature observations only.

3. Data Analysis Procedures

In this section we describe the data analysis procedure for extracting temperature fluctuations caused by gravity waves. A profile of atmospheric temperature $T(z)$ is assumed to consist of the background temperature profile $\overline{T}(z)$ and a fluctuating component $T'(z)$. We have tried to define a monthly mean profile of $\overline{T}(z)$ by averaging all of available GPS/MET data, for example, in a certain latitude band, or in the surrounding area of a specific occultation point (as defined by the tangent point of the occulted ray). Unfortunately, this produced unrealistic deviations of $T'(z)$ when we subtracted the mean profile from individual profiles. Instead, we extracted $T'(z)$ from a single GPS/MET profile by applying a high-pass filter with a cutoff at 10 km, as was done in the analysis of rocketsonde profiles [*Eckermann et al*, 1994]. We also calculated the Brunt-Väisälä frequency squared, N^2, by differentiating the temperature profile with adjacent three heights.

Figure 1 shows an example of the analyzed profiles for GPS/MET data obtained around Indonesia (11.1°S, 98.5°E) at 0418 UT on October 20, 1995. Note that the GPS/MET profiles are already low-pass filtered to reduce noise. The cutoff frequency of this filter is tuned to pass phase variations of the GPS signal corresponding to a vertical scale of 2 to 3 km in the stratosphere and approximately 200 m in the lower troposphere [*Rocken et al.*, 1997]. Accordingly, $T'(z)$ in the stratosphere consists of temperature fluctuations having a vertical scale between 2–3 km and 10 km.

We have further calculated the variance $\overline{T'^2}$ of the temperature fluctuations as

$$\overline{T'^2} = \frac{1}{z^{\max} - z^{\min}} \int_{z^{\min}}^{z^{\max}} T'^2 dz \quad (8)$$

within a layer with the top and bottom heights at $z^{\max}$ and $z^{\min}$, respectively. Note that the variance at a given altitude in Figure 1 is determined for a layer of 2 km thick, by sliding both $z^{\max}$ and $z^{\min}$ with a step of 200 m. Then, the profile of the potential energy E_p can be determined by using equation(7) with the observed N^2.

Spurious enhancements of T' can be recognized below about 10 km in Figure 1, where the effects of water vapor were ignored in deriving T. T' is suppressed in the troposphere but greatly enhanced just above the tropopause, which is generally consistent with earlier radiosonde observations [*Tsuda et al.*, 1991]. In particular, the rapid growth of $\overline{T'^2}$ across the tropopause is also reflected in a similar increase in the background N^2.

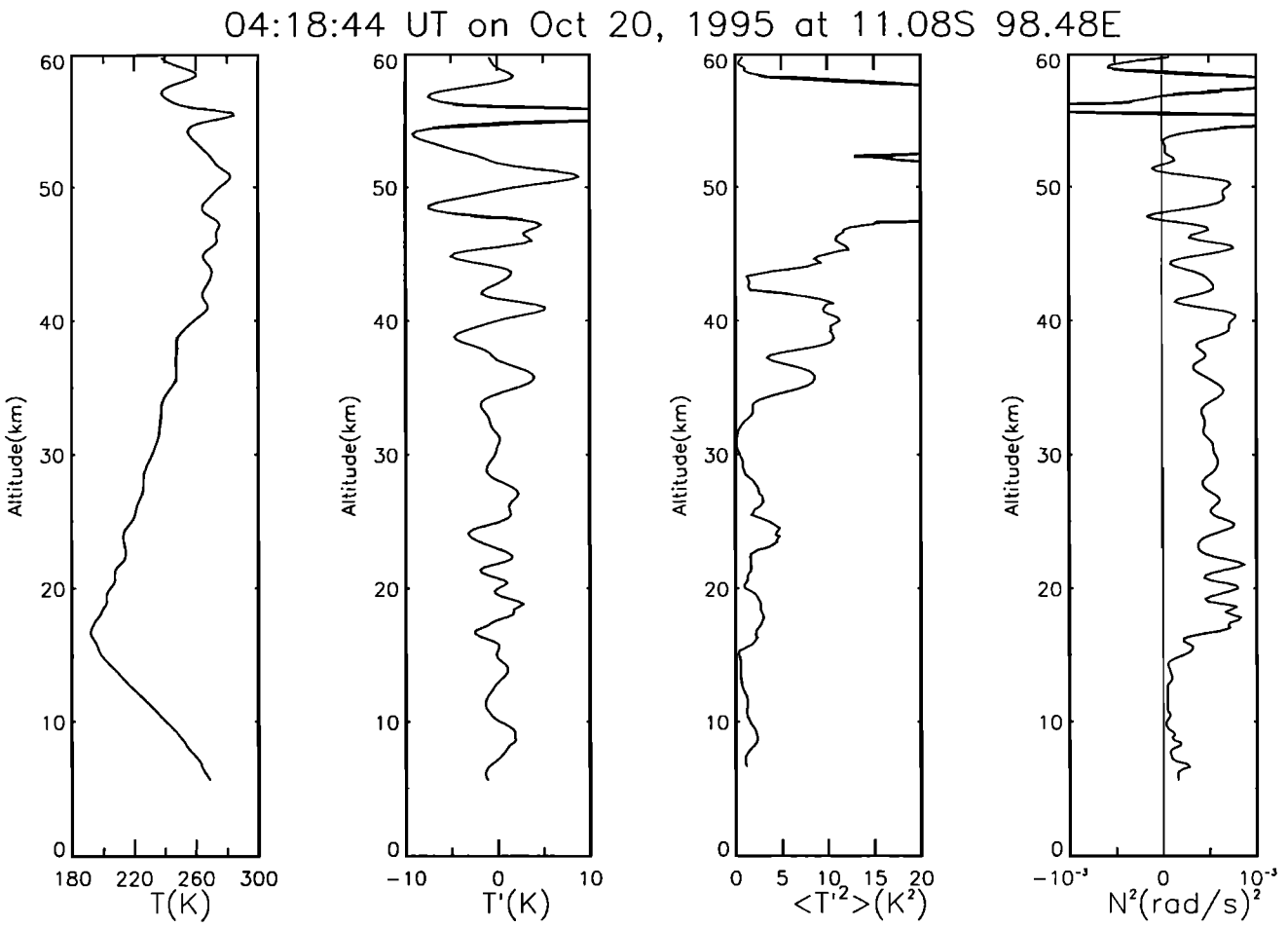

Figure 1. GPS/MET profiles obtained at (11.1°S, 98.5°E) at 0418 UT on October 20, 1995, when antispoofing (A/S) was turned off. In successive panels from left to right are original temperature T, temperature fluctuations T' after high-pass filtering with a cutoff at 10km, temperature variance $\overline{T'^2}$ in a layer with a 2 km thickness, and Brunt-Väisälä frequency squared N^2, respectively.

It is noted that part of the large T' values near 17 km in Figure 1 may be attributed to the high-pass filtering of the sharp bend in the background temperature profile near the tropopause. Therefore the temperature variance at the corresponding altitude should not be interpreted as due solely to gravity wave activity. In particular, this effect could become significant in the tropics where the temperature gradient rapidly changes near the tropopause.

The amplitudes of $\overline{T'^2}$ show an exponential increase above 30–35 km, suggesting growth of gravity wave amplitude with altitude [*Tsuda et al.*, 1994]. However, the enhanced amplitudes of T' above about 45 km are unrealistically large, compared with earlier rocketsonde results [*Tsuda et al.*, 1992; *Eckermann et al.*, 1994]. They are believed to be caused largely by residual errors in the ionospheric correction [*Rocken et al.*, 1997]. Moreover, N^2 in Figure 1 sometimes becomes negative above about 45 km, indicating a superadiabatic condition. Although small or negative N^2 can obviously be anticipated in the mesosphere due to saturation of gravity waves, the deviation of N^2 in Figure 1 is larger than expected. We suspect the large perturbations of T' above about 45 km are caused by uncertainty in the boundary condition at the top altitude or errors in the ionospheric corrections. Therefore we need to restrict the maximum height range of the analysis to about 45 km.

4. Comparison of Seasonal Variations of Gravity Wave Energy Between GPS/MET and MU Radar Observations

In this section we determine seasonal variations of E_p around Japan, using GPS/MET data, and compare the results with the climatological behavior of gravity wave kinetic energy, E_k, obtained from long-term ground-based observations with the MU radar in Shigaraki, Japan (34.9°N, 136.0°E). We have surveyed all of the GPS occultation events occurring in an area centered by Shigaraki, which extends over a latitude and longitude range of 24°–46°N and 126°–146°E, respectively.

A total of 109 GPS/MET measurements are available as shown in Figure 2. (However, three profiles were rejected, because the analyzed temperature perturbations were unrealistically large.)

A height range of 15–20 km has been selected to overlap with earlier MU radar observations of E_k [*Murayama et al.*, 1994]. From the individual GPS/MET temperature profiles we have analyzed the temperature variance defined by equation (8) for $z^{\min}$=15 km and $z^{\max}$=20 km and determined the potential energy E_p. Figure 3 shows the determined values of E_p from April 1995 to February 1997 in the top panel and the number of GPS/MET data in each month in the bottom panel. Monthly mean values of E_p with the standard deviations are also plotted in Figure 3, although the results in May and August are uncertain, since only one GPS/MET profile contributes to them. E_p was generally large in winter months and reached a minimum in summer, exhibiting an annual variation.

The tropopause in the subtropics can be as high as 15 km in summer, so the E_p values in the 15–20 km region in summer could become large due to spurious temperature perturbations produced by high-pass filtering of the sharp bend in the T profile near the tropopause. However, such effects, if exist, are not noticeable in Figures 3 and 4; therefore the E_p values seem to be correctly estimated from GPS/MET profiles.

The seasonal variation of kinetic energy E_k, caused by gravity waves, was analyzed in the lower stratosphere (15.5–17.0 km) by utilizing the results of the MU radar routine observations in 1985–1989 period [*Murayama et al.*, 1994]. In this analysis the spectral density for wind velocity frequency spectrum was integrated between the Brunt-Väisälä and the inertial frequencies, corresponding to wave periods from 5 min to 21 hours. Although a part of wave energy could spread outside of the frequency range because of the effects of Doppler shifting, reduction of E_k is not so significant for horizontal winds [*Fritts and VanZandt*, 1987]. Note also that an instantaneous profile of the GPS/MET temperature fluctuations includes all contributions from the wave frequency spectrum, so the temperature variance from the GPS/MET profiles corresponds to an integration of the spectral density for the entire frequency range.

Murayama et al. [1994] suggested that the zonal wind velocity variance $\overline{u'^2}$ shows a clear seasonal variation

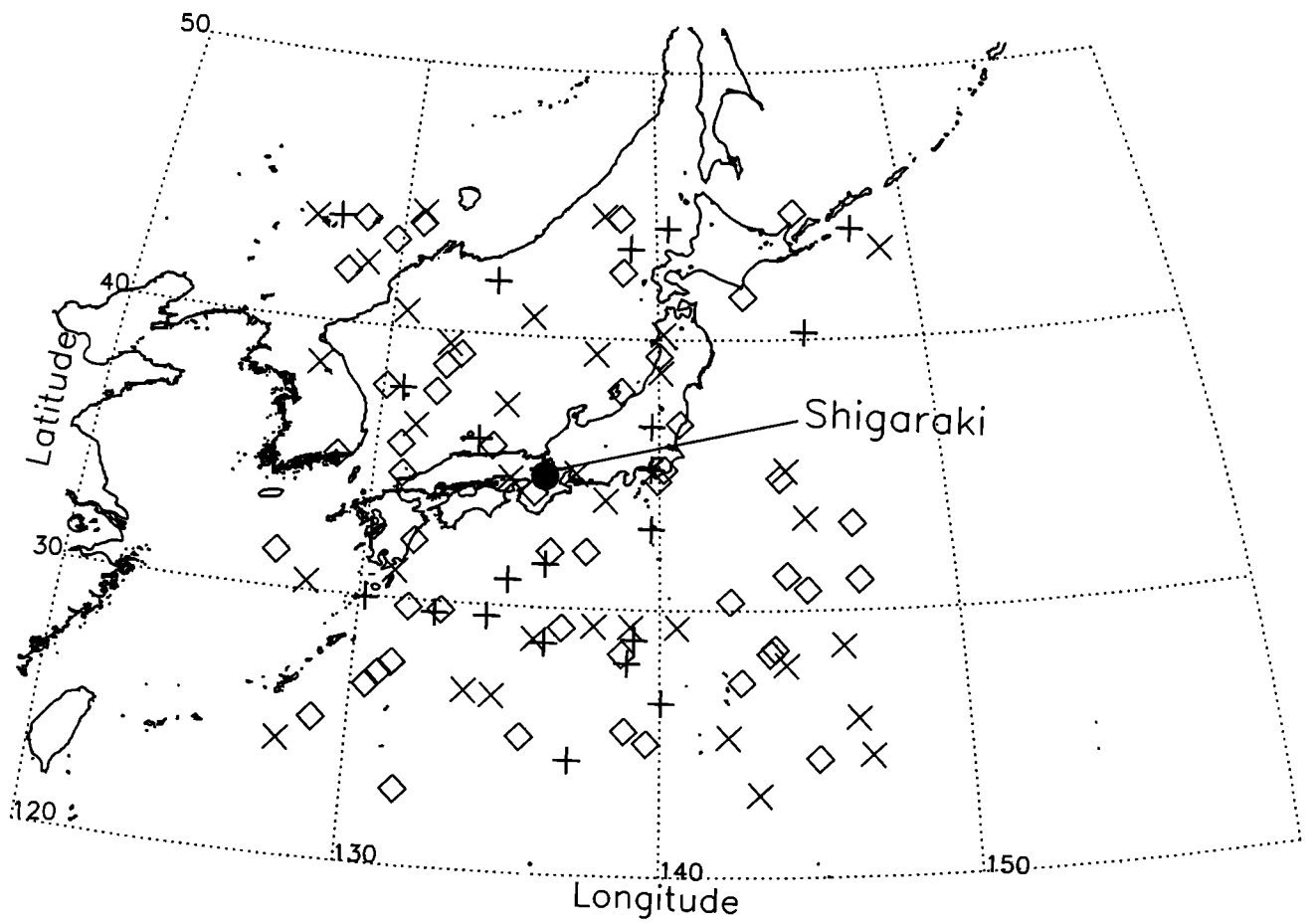

Figure 2. Locations of GPS occultation events around Japan (24°N–46°N and 126°E–146°E). Pluses, diamonds, and crosses correspond to data in 1995, 1996, and 1997, respectively. The middle and upper atmosphere (MU) radar site in Shigaraki is indicated by solid circle.

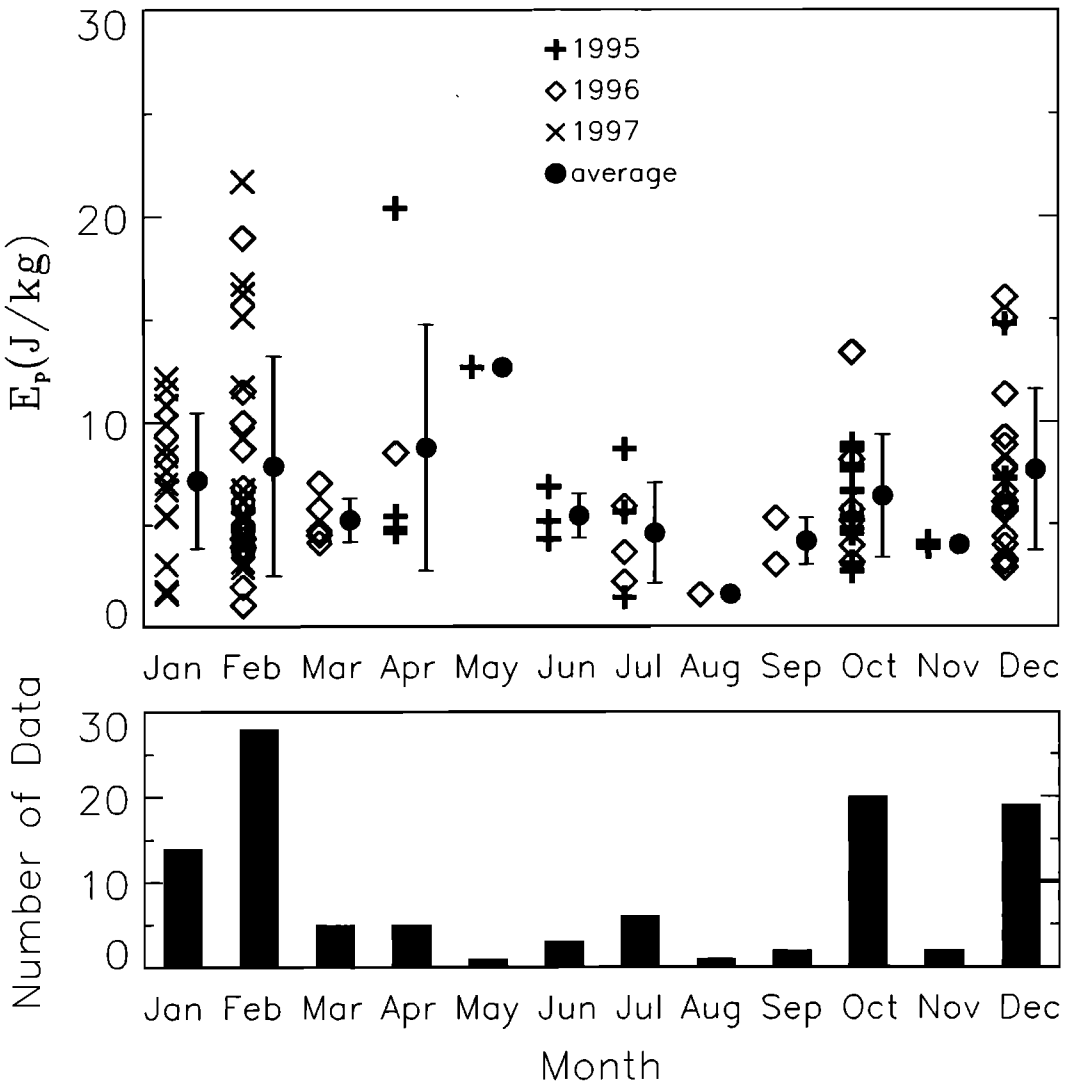

Figure 3. Determined E_p at 15–20 km from the individual GPS/MET profiles around Japan (Figure 2) is plotted for 1995 (pluses), 1996 (diamonds) and 1997 (crosses), respectively. Monthly mean of E_p together with the standard deviation are indicated by circles and a vertical bar. The number of the GPS/MET data in each month is shown by a histogram in the bottom panel.

with a maximum in December–February and a minimum in July–August in good correlation with the amplitude of the background mean winds at 12.6 km which was used as an index of the jet stream intensity. Furthermore, *Murayama et al.* [1994] reported $\overline{u'^2} \sim \overline{v'^2}$, suggesting the azimuthal isotropy of the gravity wave energy. Therefore we only need to use $\overline{u'^2}$ to calculate E_k, from equation (6).

We now compare the seasonal variations of E_k and E_p in Figure 4, derived from MU radar and GPS/MET data, respectively, where a least squares fit to the monthly mean value of E_p is illustrated in Figure 4. Both results in Figure 4 show an annual variation with a maximum in winter and a minimum in summer. The best fit sinusoidal curve in Figure 4 indicates that the E_k and E_p values range between 5–16 m^2 s^{-2} and 4–8.5 m^2 s^{-2}, respectively. Therefore the mean ratio of E_k to E_p is about 1.7.

As described in section 2, a linear theory of gravity waves predicts that E_k/E_p is p, where p is approximately 5/3(=1.67) to 2.0. Although the observed ratio for E_k/E_p is very close to a theoretical prediction, we need to investigate differences in the vertical resolution between the GPS/MET and the MU radar which could affect the quantitative comparison of E_k/E_p. The GPS/MET data extracted E_p for vertical scales ranging from 2 to 10 km, while the MU radar provided E_k for perturbations with a vertical scale larger than 300 m.

To estimate the effects of the difference in the vertical resolutions between the MU radar and the GPS/MET, we employ a model vertical wavenumber spectrum defined by equation (4). Figure 5 shows the model power spectrum with $1/m_* = 3$ km in an area-preserving form in which the area below the spectrum is proportional to the wave energy. Taking the higher cutoff for the GPS/MET to be about 5×10^{-4} cycles m^{-1} (2 km in vertical wavelength), we have calculated the energy E_{GPS} for GPS/MET sounding by integrating the spectrum in Figure 5 over a wavelength range between 2 and 10 km. For E_{MU} (the MU radar energy) the spectrum

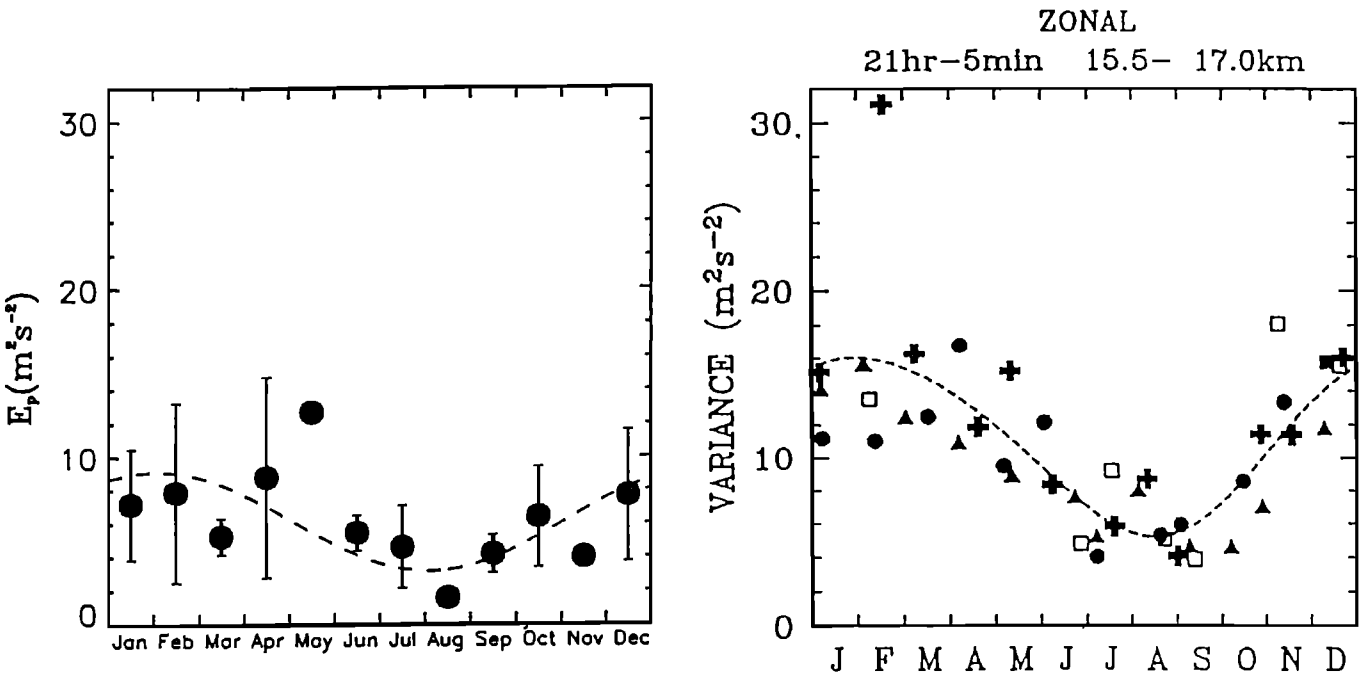

Figure 4. Comparison between E_k at 15.5–17.0 km observed with the MU radar (left; reproduced from *Murayama et al.* [1994]) and the monthly average value of E_p with the GPS/MET data (right; replotted from Figure 3). The dashed line indicates a least squares fit of E_k and E_p.

is integrated over wavelengths longer than 300 m. The model results predict E_{GPS}/E_{MU}=0.68. Given that E_p in Figure 4 could be underestimated by this factor, the ratio E_k/E_p may be reduced to 1.2. Note, however, that the ratio could deviate depending on the model parameters; moreover, the filter pass bands are not ideal as assumed in Figure 5.

Because the horizontal resolution of the GPS/MET sounding is roughly 300–500 km in the stratosphere [*Melbourne et al.*, 1994], part of the horizontal inhomogeneity of the temperature field is smoothed out, and the E_p, due to small horizontal scale gravity waves, is removed. This reduction of E_p can be estimated by assuming a horizontal wavenumber spectrum proportional to $k^{-5/3}$ between the respective maximum and the minimum horizontal wavelengths, λ_x^{max}=5000 km and λ_x^{min}=1 km. Assuming the observational limit in λ_x with GPS/MET is 300–500 km, the E_p obtained with GPS/MET is reduced by about ~15–21%.

It is noteworthy that a similar comparison has been conducted between the GPS/MET results and the Stratosphere troposphere (ST) radar observations at White Sands Missile Range, New Mexico (32.41°N, 106.35°W), which reports a good consistency of the seasonal variations between E_p and E_k as well as their energy ratio [*Nastrom et al.*, 1999]. Thus the utilization of the GPS/MET profiles in the study of stratospheric gravity wave activity has been verified at these specified radar sites.

To summarize, this comparison implies that GPS/MET data in the stratosphere can be used to extract E_p for the mesoscale temperature perturbations with a vertical scale ranging from 2 to 10 km, which are presumably caused by gravity waves. In section5 we further study the distribution of gravity wave activity as a function of latitude, longitude, altitude, and season by taking advantage of the global coverage of the GPS/MET data.

5. Global Distribution of Gravity Wave Activity at 20–30 km from November to February

We separated a year into four seasons, i.e., March to April, May to August, September to October, and November to February. Then, using equations. (7) and (8), we have analyzed E_p from the individual GPS/MET temperature profiles, collected from April 1995 to February 1997 [*Rocken et al.*, 1997]. First, we have determined the latitude-longitude distribution of E_p in the 20–30 km height region in the Northern Hemisphere winter months (from November to February), when the largest number of GPS/MET profiles were collected (a total of 4569 out of 10,853) [*Rocken et al.*, 1997]. Figure 6 shows a distribution of the occultation events in November–February. Note that only few data points were obtained around tropical Africa. A larger amount of data was collected at middle and high latitudes due to the configuration of the satellite orbits and the distribution of the ground reference sites.

5.1. A Longitude-Latitude Distribution of E_p

We have averaged individual E_p values over 20° in longitude and 10° in latitude, while the coordinates of the center are shifted every 1° and 2° along latitude and longitude, respectively. We have rejected some unreal-

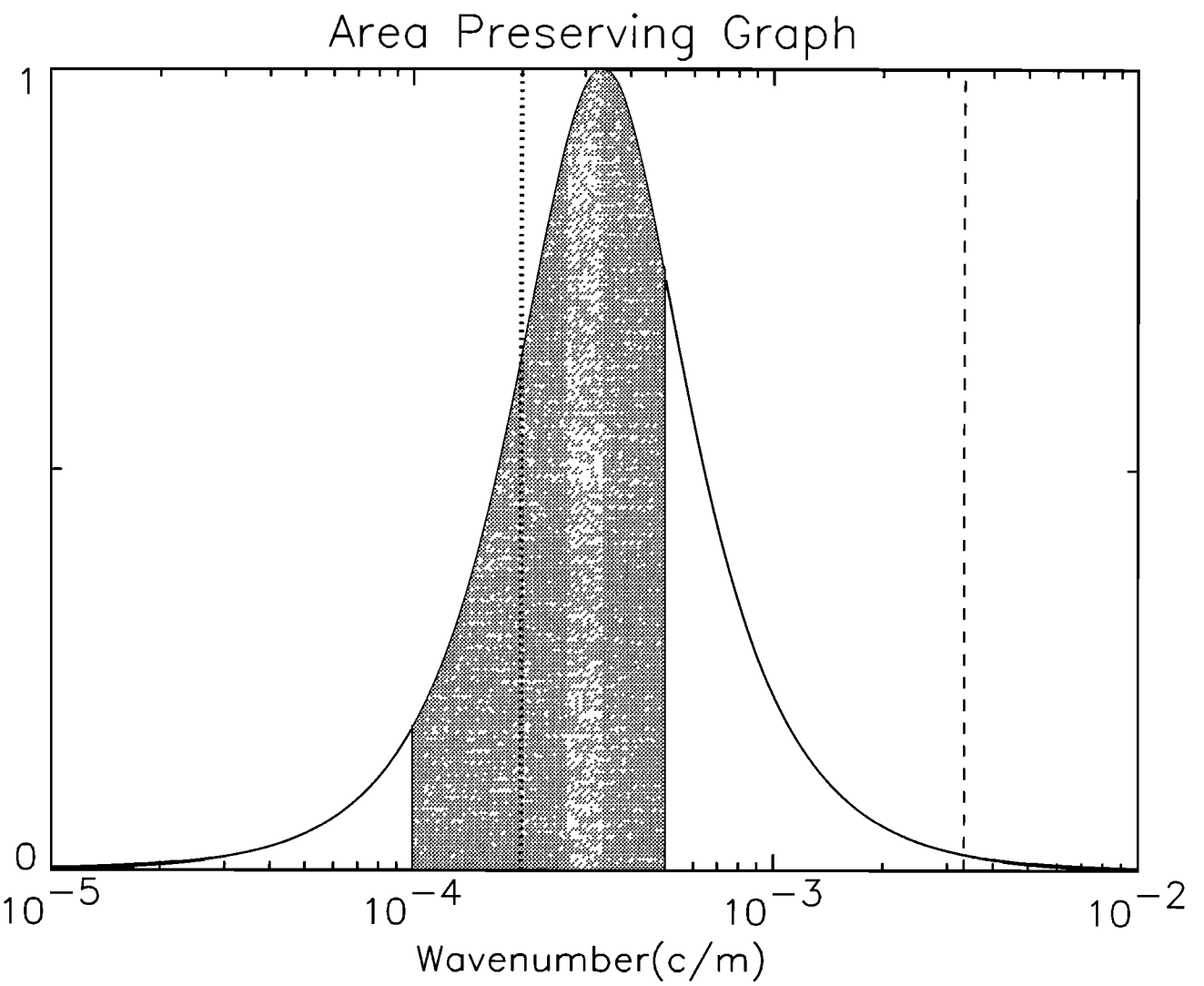

Figure 5. A model vertical wavenumber spectrum with a characteristic wavelength $(1/m_*)$ of 3 km in an area-preserving form is plotted along with a vertical dashed line at 1/300 cycles m^{-1} corresponding to the height resolution for the MU radar measurements. The shaded area indicates the wavenumber range for GPS/MET data (2–10 km in vertical wavelength), and a dotted line corresponds to 5 km in vertical wavelength.

istic profiles (about 2.5% of total data), when $\overline{T'^2}$ values exceeded 15 K^2. Plate 1 shows the global distribution of E_p at 20–30 km in November–February.

Large E_p values (exceeding 6 J kg^{-1}) are mostly detected at low latitudes from 25°N to 25°S centered around the equator, and they are particularly enhanced over the regions where active convection is expected, such as over the Indonesian archipelago, the Indian Ocean, eastern Atlantic Ocean, and South America. The E_p values at midlatitudes (higher than 30°) are generally larger in the Northern (winter) Hemisphere.

Plate 1 strongly suggests that atmospheric waves are actively generated by tropical convection. However, our analysis using instantaneous temperature profiles cannot accurately estimate the relative significance of the contributions to E_p between gravity waves and planetary-scale equatorial waves, such as Kelvin waves and mixed Rossby gravity waves. As a matter of fact, E_p in Plate 1 is much larger in the tropics than in the midlatitudes of the winter hemisphere where gravity waves are efficiently generated by orographic effects and meteorological disturbances [e.g., *Nastrom and Fritts*, 1992; *Fritts and Nastrom*, 1992]. In the following we aim at estimating the extent that Kelvin waves and other equatorial waves contribute to the large E_p values at low latitudes.

It is plausible to assume that the equatorial wave field at the fairly low altitudes in the stratosphere is dominated by longer horizontal wavelengths and lower-frequency components [e.g., *Andrews et al.*, 1987]. Then, the equatorial waves most likely produce the zonally symmetric component of E_p near the equator. If equatorial waves indeed dominate the E_p pattern in Plate 1, the longitudinal inhomogeneity would be expected to

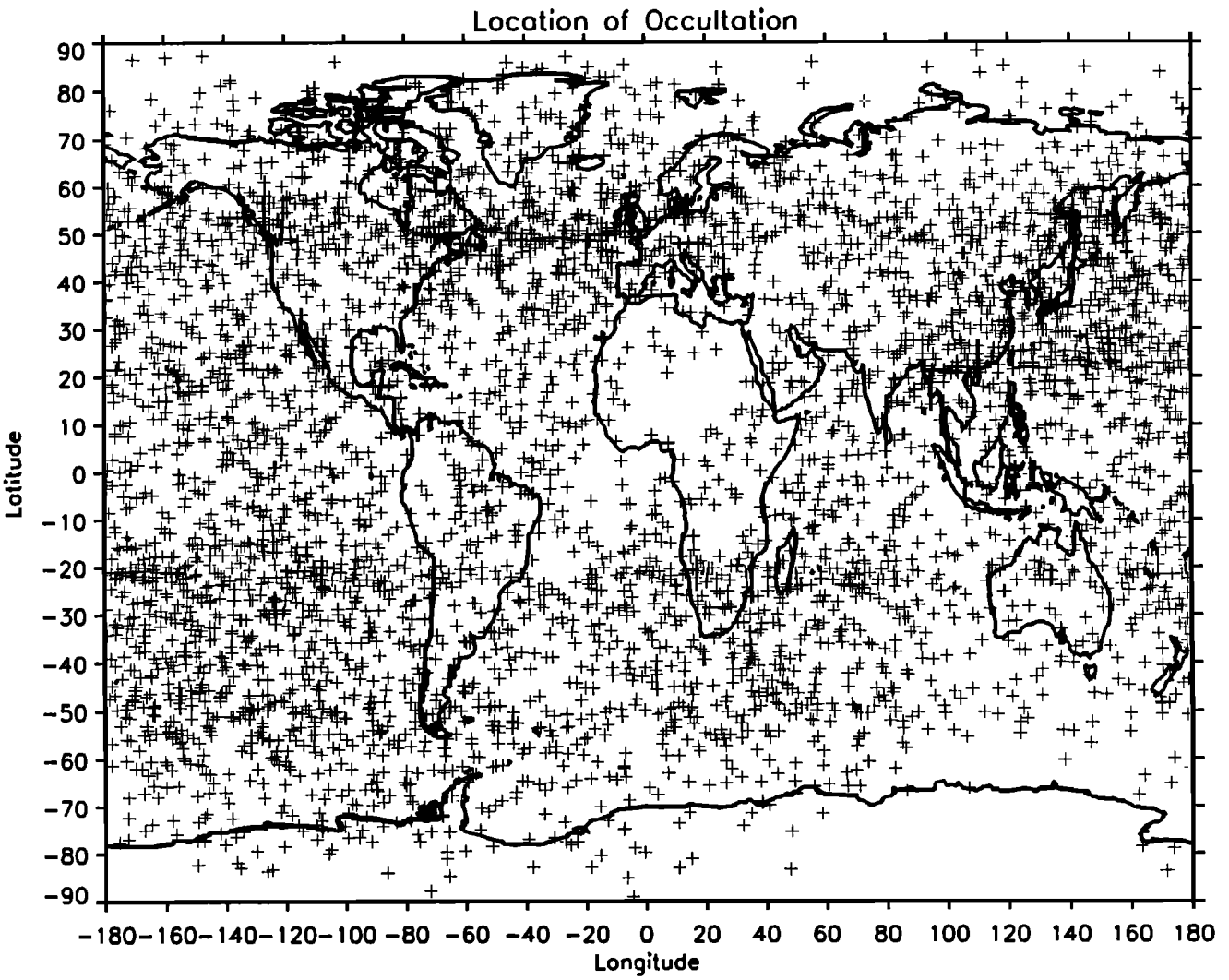

Figure 6. Distribution of about 4500 GPS/MET profiles during Northern Hemisphere winter (from November to February). Both A/S-on and A/S-off data are included.

be less pronounced. Therefore the detailed latitude-longitude distribution in Plate 1 seems to reflect the localized excitation of gravity waves. It is noteworthy, however, that high-frequency Kelvin waves with a broader horizontal wavenumber spectrum can be generated by any localized forcings, which could produce longitudinal inhomogeneity and latitudinal asymmetry as seen in Plate 1.

Eckermann et al. [1994] investigated contamination of Kelvin waves into the gravity wave analysis in equatorial regions from rocketsonde profiles by means of a high-pass filter with a cutoff at 10 km and concluded that the zonal alignment of the analyzed wave propagation direction indicates a predominance of Kelvin waves. However, recent analysis with high-resolution radiosondes in Indonesia has determined the dominance of gravity waves in the lower stratosphere, which preferentially propagate zonally due to interaction with the quasi-biennial oscillation (QBO) [*Shimizu and Tsuda*, 1997].

The latitude variation of equatorial waves with a vertical wavenumber m can be approximated by a Gaussian distribution about the equator with an e-folding width given by $\sigma = \sqrt{\beta|m|/2N}$, where β is the latitudinal gradient of the Coriolis parameter [*Andrews et al.*, 1987]. Substituting $m = 2\pi/10$ rad km^{-1}, which corresponds to the smallest m in our analysis, we get $1/\sigma$=1700 km, or about 15° in latitude. Then, the e-folding width for the variance becomes about 11°. Therefore equatorial waves with vertical scales smaller than 10 km seem mostly be confined to about ±10°–15° around the equator. Plate 1 indicates that the extent of the large E_p values is wider than expected for equatorial waves. Using the same relation, *Eckermann* [1995] investigated the meridional extent of equatorial waves with rocketsonde data and reported that the wave energy in the 2–20 km vertical scale was dominated by equatorial waves at 20–40 km altitude. However, in the 2–10 km band of vertical wavelengths, predominance of equatorial waves was not evident, instead, it was suggested that gravity waves significantly contribute to the wave energy.

We have reanalyzed E_p, reducing the cutoff of the high-pass filter from 10 km to 5 km (2–5 km pass-

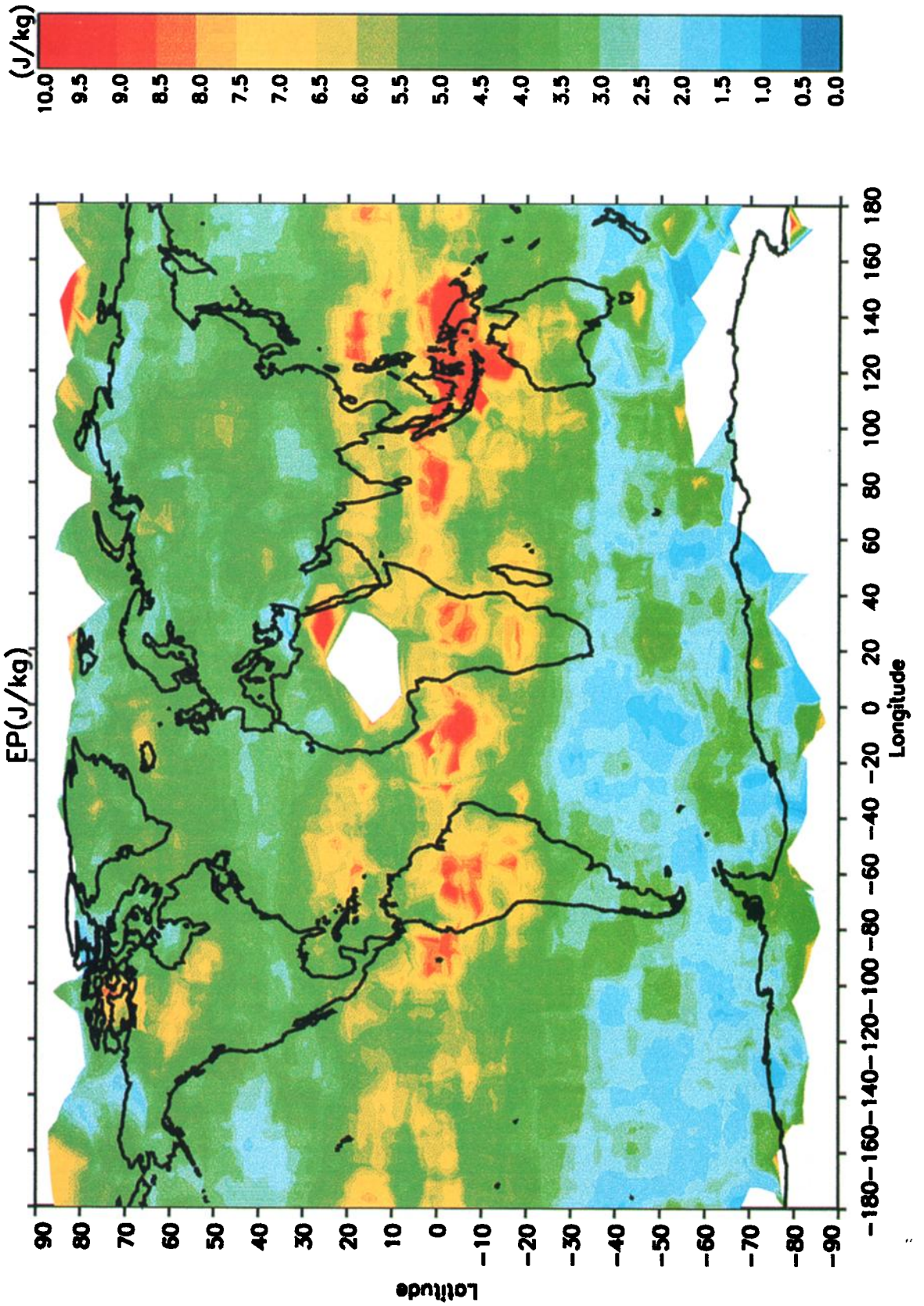

Plate 1. Global distribution of E_p from the GPS/MET data at 20–30 km in November–February. The E_p value is averaged in an area extending 10° and 20° in latitude and longitude, and the center coordinates are shifted every 1° and 2°, respectively.

band) in determining the temperature variance (figure not shown) and found that the latitude extent of large E_p is slightly reduced, although the fundamental pattern of E_p is not significantly modified. It is noteworthy that the enhancement of E_p is very clearly concentrated over Indonesia (100°–150°E, 10°N–10°S), and the other smaller enhancement appears over the Atlantic Ocean (0°–30°W, 0°–10°S). The magnitude of the reanalyzed E_p, however, becomes about half of the values plotted in Plate 1, although we could expect the reduction of E_p by about 24%, if we change the filter passband of the vertical wavenumber spectrum in Figure 5 from 2–10 km to 2–5 km. Therefore E_p in Plate 1 does not seem to be contributed solely by gravity waves, and it obviously includes additional energy due to equatorial waves.

To summarize, Plate 1 indicates that temperature perturbations with a vertical scale ranging from 2 to 10 km are the largest at low latitudes, which seems to be generated by tropical convections. However, this analysis without wind velocity measurements is unable to distinguish small-scale gravity waves from planetary-scale equatorial waves. Therefore the E_p values at low latitudes in Plate 1 could partially be contributed by equatorial waves that are most likely to add a zonally symmetric bias. At middle and high latitudes the latitude-longitude variations of E_p in Plate 1 seems to represent the global distribution of gravity wave activity in the lower stratosphere, which is larger in the winter (northern) hemisphere.

5.2. Longitude Variations of E_p in the Midlatitudes

We have also analyzed longitudinal distributions of E_p at 20–30 km from November to February for the evaluation of orographic effects, as shown in Figure 7. Since we are interested in the differences in E_p between continents and oceans (orographic effects), we have focused on a latitude band from 30°N to 60°N where the topography can be classified into continents (65°–130°W and 0°–145°E) and oceans (0°–65°W and 130°W–145°E) as indicated in Figure 7. There is a tendency for E_p in Figure 7 to be larger over continents than over oceans. In particular, E_p was enhanced over North America, while it was depressed in the central Pacific.

We have also analyzed longitude variation of E_p at 20–30 km in a latitude band from 10°S to 40°S in May–August (winter months in the Southern Hemisphere) and found larger E_p values (about 4 J kg^{-1}) over South America (figure not shown), while E_p values were smaller (about 3 J kg^{-1}) in the Pacific and Atlantic Oceans. Enhancement of E_p ranging 3.5–4 J kg^{-1} was also recognized around Africa and Australia, although the longitude variation did not clearly reflect the land-sea distribution.

These land-sea contrasts in E_p could be attributed to the effects of mountain lee waves caused by an interaction between topography and surface winds [*Nastrom and Fritts*, 1992]. However, the distribution of topography may not directly be reflected into the stratospheric E_p pattern, because gravity waves could propagate for a great horizontal distance from the region of generation. Moreover, interactions of gravity waves with the background wind and stability fields largely affect the vertical wave propagation characteristics, and therefore the E_p pattern could largely be modified [*Alexander*, 1998].

6. Latitude and Height Variations of E_p between 15 and 45 km

Since we restricted the maximum height for the gravity wave analysis to 45 km we have selected a height range between 15 km and 45 km, and defined five overlapping height regions with a 10 km thickness starting from 15 km and an increment of 5 km. It is noteworthy that the noise on the L2 band of GPS signals considerably increased when antispoofing (A/S) encryption of the GPS signals was turned on [*Rocken et al.*, 1997]. Then, effects of ionospheric correction produce artificial fluctuations in the GPS/MET temperature profiles, which could be recognized down to about 30 km. Therefore we used only data during prime times under A/S-off conditions for a study of the height variations of E_p distributions.

6.1. Latitude Variation of E_p

Figure 8 shows latitudinal variations of E_p in the five altitude ranges, where individual E_p values are averaged every 10° in 18 latitude bands. Note that the results in March–April are not shown here because the number of GPS/MET profiles under A/S-off conditions was insufficient (430), while 1608, 1430, and 1836 profiles were used in May–August, September–October, and November–February, respectively. The latitudinal distribution of the GPS occultation events, as shown in a histogram in Figure 8, is nearly symmetric relative to the equator, with the maximum around 30° in each hemisphere. However, it was significantly reduced at latitudes higher than 70°. Therefore, the analyzed results in the polar regions may not be statistically significant.

Table 1 summarizes the E_p values in the three seasons at 20–30 km and 30–40 km at 40°–60°N, 10°S–10°N and, 40°–60°S. The corresponding normalized temperature variance $\overline{(T'/\overline{T})^2}$ is also listed in parentheses. Had we analyzed the E_p values, using all available data including A/S-on, the results at 30-40 km would show an increase in E_p by about 1.4 J kg^{-1} (about 30 %) due to increased noise in the A/S-on data. However, fundamental structure of the latitude distribution of E_p is not largely modified from Figure 8 except for a constant bias, although the standard deviation for each E_p determination greatly increases. If A/S-on data were included, the increase in E_p at 20-30 km would be as small as 0.2 J kg^{-1} (about 5 %), and the latitude distributions of E_p below 30 km are very similar to those in Figure 8.

In the lowest two layers below 30 km (15–25 km and 20–30 km) in Figure 8, we have detected the largest

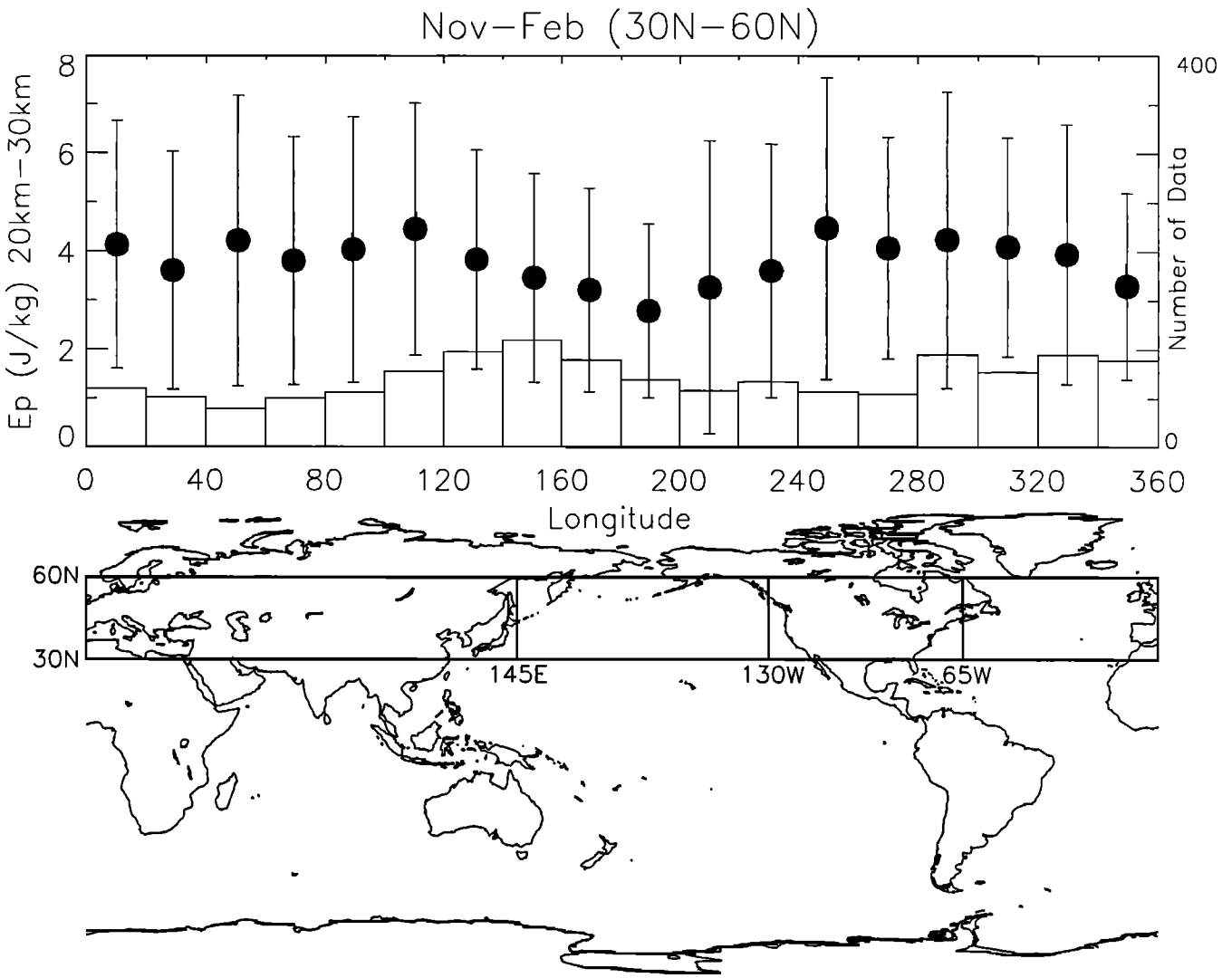

Figure 7. Longitudinal variations of E_p at 20–30 km in a latitude range between 30°N and 60°N during winter months (November to February), averaged every 20° in 18 longitudinal sectors. The number of data points in each sector is shown by a histogram, and the regions of continents and oceans are divided in the bottom panel.

value of E_p in the low latitudes, as already recognized in Plate 1, where the latitude range of the enhanced E_p is wider in November–February than in other seasons. However, it is noteworthy that the tropopause is generally located at 16–17 km in the tropics, so the E_p values in the 15–25 km region in Figure 8 could be affected by the temperature structure near the tropopause, as discussed in section 2. Therefore it is inappropriate to interpret the E_p values at 15–25 km in terms of wave activities at low latitudes (30°N–30°S). On the other hand, the large E_p values in the tropics in the 20–30 km region seems to be a manifestation of atmospheric wave activity.

In the 20–30 km layer the E_p values at midlatitudes are larger in the winter hemisphere, which is more evident in May–August, while in equinox (September–October), E_p in the midlatitudes is nearly the same between the Northern and the Southern Hemispheres. Above 30 km the enhanced peak of E_p near the equator tends to disappear, but the E_p at higher latitudes becomes larger, which is consistent with the shuttle experiment of stratospheric gravity wave activity [*Preusse et al.*, 1998].

It is remarkable that in September–October the latitudinal distribution of E_p is symmetric between the Northern and the Southern Hemispheres in the entire height ranges. However, near solstices the E_p distribution involves a large hemispheric asymmetry at middle and high latitudes, which is more pronounced in May–August. There are also differences in the E_p distribution between the June and the December solstices. For example, E_p values at 40°–70°S in May–August are significantly larger than those at 40°–70°N in November–February. Conversely, E_p values at 40°–70°S in November–February are smaller than those at 40°–70°N in May–August. These results suggest that

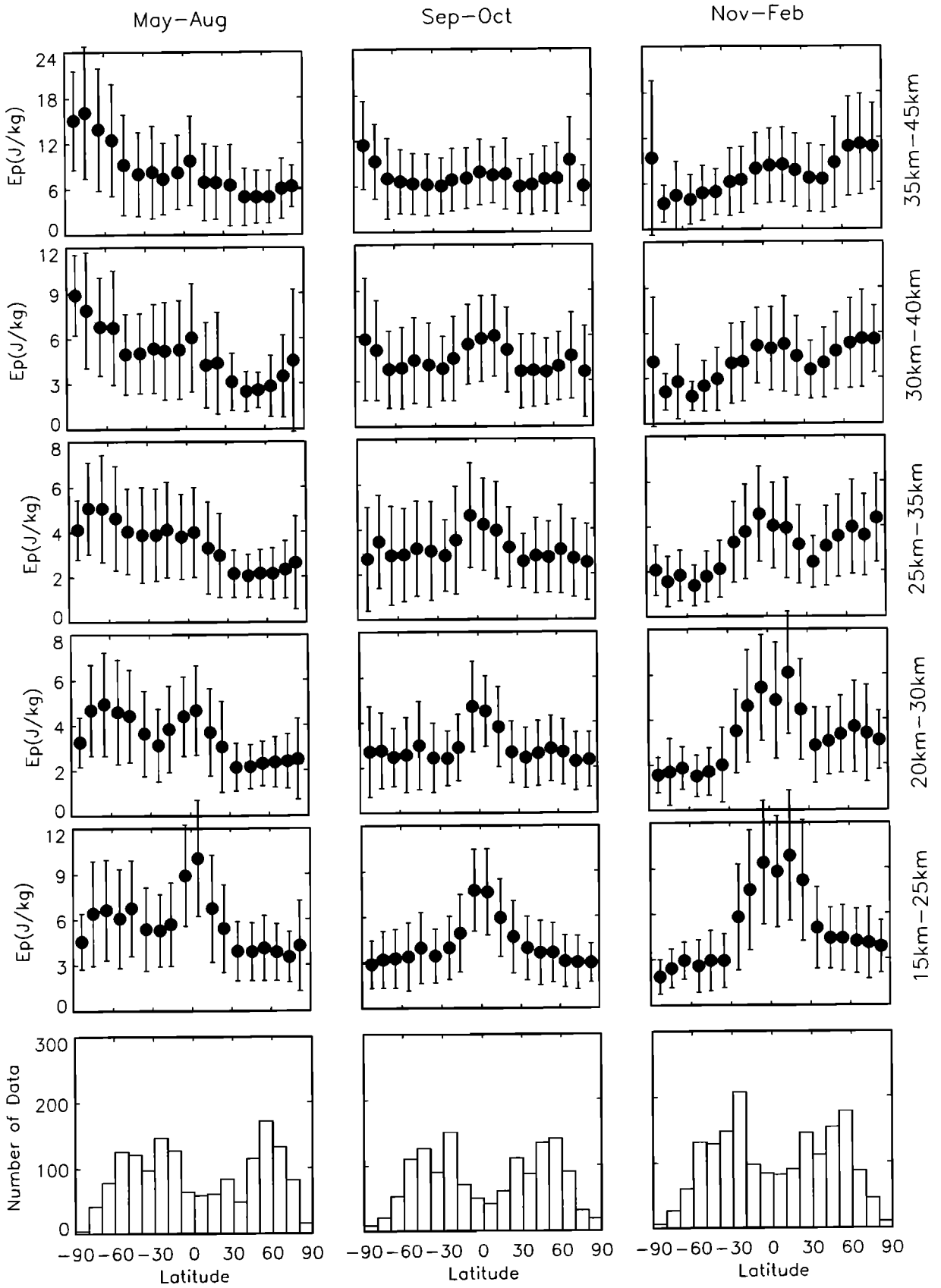

Figure 8. Latitudinal variations of the zonally averaged E_p and standard deviation in five altitude regions in November–February (right), September–October (middle), and May–August (left). Number of GPS/MET data is shown in a histogram. Only A/S-off data are used.

Table 1. E_p and $\overline{(T'/\overline{T})^2}$ Estimates From GPS/MET Profiles

	May–Aug., E_p, J kg^{-1}	$\overline{(T'/\overline{T})^2}$, %^{2}	Sept.–Oct., E_p, J kg^{-1}	$\overline{(T'/\overline{T})^2}$, %^{2}	Nov.–Feb., E_p, J kg^{-1}	$\overline{(T'/\overline{T})^2}$, %^{2}
			40°–60°N			
30–40 km	2.5	(0.26)	3.5	(0.36)	4.5	(0.47)
20–30 km	2.2	(0.21)	2.6	(0.26)	3.1	(0.29)
			10°S–10°N			
30–40 km	5.5	(0.55)	5.5	(0.58)	5.1	(0.53)
20–30 km	4.9	(0.54)	5.1	(0.57)	5.9	(0.69)
			40°–60°S			
30–40 km	6.0	(0.70)	4.7	(0.49)	2.1	(0.21)
20–30 km	4.5	(0.42)	3.1	(0.31)	1.5	(0.25)

the latitudinal distribution of the gravity wave activity in the stratosphere depends on hemisphere as well as on season.

Both the hemispheric asymmetry and the differences between the June and the December conditions were also reported by *Wu and Waters* [1996a, b], based on gravity wave analysis from the UARS-MLS measurements. However, a direct comparison with our results is not discussed here, because the height and latitude ranges of the major variations do not overlap each other. Moreover, the UARS/MLS observed waves with a vertical scale larger than about 10 km, so there is little overlap in wavelength ranges with the present study using the GPS/MET profiles.

Eckermann et al. [1994] extracted fluctuations of temperature and horizontal wind velocity in the 20–60 km height range from rocket soundings during 1977–1987 at 15 stations, mostly distributed in the Northern Hemisphere. A filter was applied on individual profiles with a 2–10 km passband, then a normalized temperature variance $\overline{(T'/\overline{T})^2}$ was determined, which can directly be compared with the GPS/MET results in Table 1. *Eckermann et al.* [1994] reported that at middle and high latitudes (38°N, 55°N and 59°N) $\overline{(T'/\overline{T})^2}$ in the altitude range of 20–40 km showed a clear annual variation with a minimum (0.3–0.4 %^{2}) in summer and a winter maximum (0.7–1.0 %^{2}). From Table 1 we can determine the $\overline{(T'/\overline{T})^2}$ values at 40°–60°N in the 20–40 km region as 0.24, 0.31, and 0.38 %^{2} in summer, equinox, and winter, respectively, which is a factor of 0.5–0.7 compared to the rocketsonde results, although the seasonal variation in the northern midlatitudes is generally consistent with the rocketsonde analysis. *Eckermann et al.* [1995] explained the annual cycle of $\overline{(T'/\overline{T})^2}$ in terms of the variation in density scale height, which may also explain the GPS/MET derived seasonal variations.

Allen and Vincent [1995] determined E_p at 17–24 km altitude from radiosonde soundings over Australia and reported a seasonal variation of E_p at midlatitudes, having a maximum value of 6–7 J kg^{-1} in winter and a minimum value of less than 5 J kg^{-1} in summer. While the GPS/MET results at 15–25 km in Figure 8 indicate 5–6 J kg^{-1} in winter (May-August) and about 3 J kg^{-1} in summer months (November–February), which are consistent with the radiosonde analysis. It is noteworthy, however, that the GPS/MET data generally detected slightly smaller E_p values than the balloon results, probably because of the poorer height resolution and averaging over a horizontal area, as discussed in section 4.

6.2. Height Variation of E_p

Figure 9 shows a height profile of E_p in the three seasons at 40°–60°N, 10°S–10°N, and 40°–60°S. Each E_p value is determined in five layers between 15 and 45 km with a thickness of 10 km.

In the 40°–60°N region the E_p value decreases with altitude to a minimum around 25–30 km and after which it increases with altitude. An annual variation with a maximum in winter is evident above 25 km, and the relative height variations are similar among the three seasons, which is consistent with the rocketsonde results, for example, at Primrose Lake (55°N, 110°W) [*Eckermann et al.*, 1994].

Although the general structure of each height variation of E_p at 40°–60°S is similar to that in the Northern Hemisphere, large hemispheric differences can also be recognized. In particular, the annual variation of E_p is considerably enhanced over all heights in the Southern Hemisphere. As discussed in section 6.1 concerning Figure 8, the large winter-summer difference in E_p in the Southern Hemisphere is observed at latitudes higher than about 40°S.

In the equatorial region, height profiles overlap each other without a significant seasonal variation. Although the large E_p values were observed at 20 km (15–25 km region), they may be affected by the spurious temperature perturbations caused by a filtering of sharply bent temperature profiles near the tropopause located at 16–17 km. So the E_p values at 20 km should not be interpreted as the gravity wave energy in the tropics. The

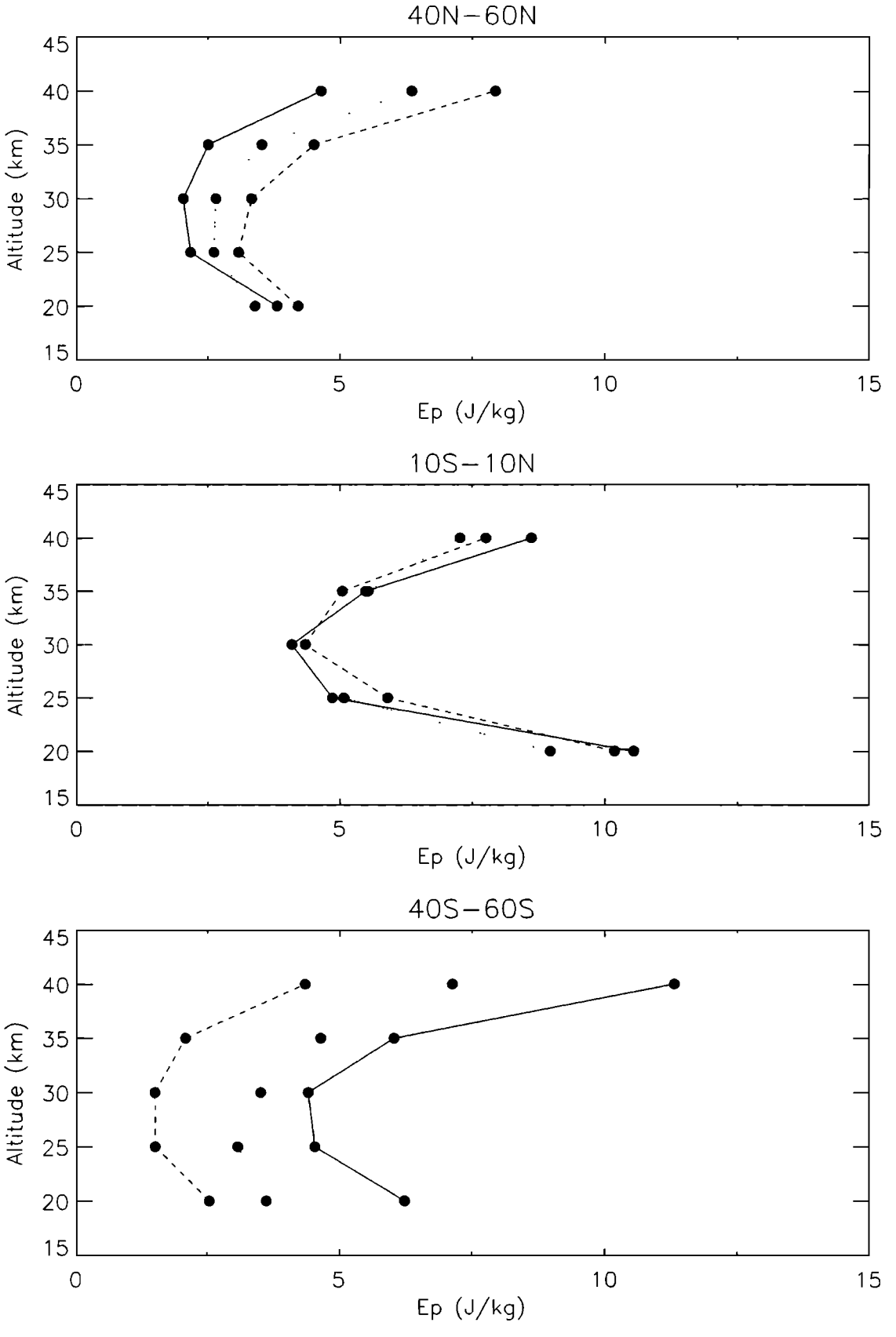

Figure 9. Height variation of the zonally averaged E_p with a standard deviation at 40°–60°N (top), 10°S–10°N (middle), and 40°–60°S (bottom), respectively. Solid, dotted, and dashed lines correspond to the results during May and August, September and October, and November and February, respectively. Only A/S-off data are used.

E_p values sharply decreases at 25–30 km, but the rate between 30 and 35 km is nearly equal to that in the northern midlatitudes.

7. Summary

Profiles of atmospheric temperature in the upper troposphere and stratosphere between April 1995 and February 1997 have been obtained by the GPS/MET (GPS Meteorology) experiment from radio occultation observations of GPS (Global Positioning System) signals. From a single GPS/MET profile we have extracted temperature perturbations with vertical wavelength scales ranging from 2 to 10 km and derived potential energy E_p with the local N^2 values, which are also estimated from the GPS/MET results.

We have determined monthly mean values of E_p at 15–20 km altitude around Japan (24°–46°N, 126°–146°E) and found a seasonal variation with an enhancement in winter months. The results agree very well with the climatological behavior of E_k due to the gravity wave observed with the MU radar in Shigaraki during 1985–1989. It is noteworthy that the ratio of E_p to E_k agrees reasonably well with a theoretical prediction assuming linear gravity waves, although the effects of the difference in the vertical and horizontal resolutions between GPS/MET and the MU radar measurements should be investigated in more detail.

Taking advantage of the global coverage of the GPS/MET data, we have analyzed the latitude-longitude distribution of E_p at 20–30 km during the Northern Hemisphere winter (from November to February) when the largest number of GPS/MET profiles were available. The largest E_p values are generally centered around the equator between 25°N and 25°S, and they are particularly enhanced over the Indonesian archipelago, the Indian Ocean, Africa and the Atlantic Ocean to its west, and South America. This result strongly suggests that atmospheric waves are generated by convection in the tropical regions. However, this study, using only instantaneous temperature profiles, is difficult to distinguish small-scale gravity waves from planetary-scale equatorial waves. Therefore the E_p in the tropics so determined may include the effects of equatorial waves that could add a zonally symmetric bias.

Longitudinal variations of E_p at 20–30 km are determined in a latitude range of 30°–60°N from November to February. We have found a tendency for E_p to become larger over the continents than over the Pacific Ocean, possibly suggesting orographic generation of mountain lee waves due to interaction between mean winds and topography.

The highest quality E_p estimates above 30 km were obtained when GPS/MET was operated in a mode without antispoofing. Using these data without antispoofing, latitudinal variations of E_p were determined for several altitude layers with a thickness of 10 km between 15 and 45 km altitude. The results indicate that large E_p values are concentrated near the equator at 20–30 km. However, there is a tendency for E_p to become larger at midlatitudes at 30–40 km and higher altitudes. The gravity wave activity at midlatitudes was generally larger in winter months in both hemispheres, although differences do exist between Northern and Southern Hemispheres. During equinoxes, a remarkable latitudinal symmetry of E_p relative to the equator was found.

We have determined height variations of E_p in the equatorial region (10°S–10°N) and at midlatitudes (40°–60°). The E_p values decrease between 20 km and 25–30 km altitude and show a gradual and rapid increase at 25–35 km and above 35 km, respectively. A strong annual variation with maximum in the winter is again detected in both Northern and Southern Hemispheres, although large hemispheric differences are recognized. On the other hand, seasonal variations are not evident in the equatorial region. This study has clarified that the GPS occultation technique provides important and unique data sets for the study of global distribution of atmospheric gravity waves.

Acknowledgments. The GPS/MET program is sponsored primarily by the National Science Foundation (NSF), and temperature profiles derived from the GPS occultation measurements were provided by the UCAR GPS/MET office. This study is supported by the Japanese GPS-Meteorology project of Science and Technology Agency (STA), Japan. We thank D. C. Fritts and friends in Boulder for helpful conversations during a visit with T.T. and M.N. at Colorado Research Associates (CoRA). We are particularly grateful to C.-Y. She and D. M. Riggin for helpful comments and careful reading of the manuscript. Discussions and correspondence with G. Nastrom, T. E. VanZandt, I. Hirota, S. Yoden, and M. Shiotani are gratefully acknowledged. We especially wish to thank M.-L. Chanin and M. A. Geller for helpful suggestions at the SPARC-SSG meeting in October 1998 in Nagoya.

References

Alexander, M. J., Interpretations of observed climatological patterns in stratospheric gravity wave variance, *J. Geophys. Res.*, *103*, 8627–8640, 1998.

Alexander, M. J., and J. R. Holton, A model study of zonal forcing in the equatorial stratosphere by convectively induced gravity waves, *J. Atmos. Sci.*, *54*, 408–419, 1997.

Alexander, M. J., and L. Pfister, Gravity waves momentum flux in the lower stratosphere over convection, *Geophys. Res. Lett.*, *22*, 2029–2032, 1995.

Allen, S. J., and R. A. Vincent, Gravity wave activity in the lower atmosphere: Seasonal and latitudinal variations, *J. Geophys. Res.*, *100*, 1327–1350, 1995.

Andrews, D. G., J. R. Holton, and C. B. Leovy, *Middle Atmosphere Dynamics*, Academic, San Diego, Calif., 1987.

Desaubies, Y. J. F., Analytical representation of internal wave spectra, *J. Phys. Oceanogr.*, *6* , 976-981, 1976.

Eckermann, S. D., On the observed morphology of gravity-wave and equatorial-wave variance in the stratosphere, *J. Atmos. Sol. Terr. Phys.*, *57*, 105–134, 1995.

Eckermann, S. D., I. Hirota, and W. K. Hocking, Gravity wave and equatorial wave morphology of the stratosphere derived from long-term rocket soundings, *Q. J. R. Meteorol. Soc.*, *121*, 149–186, 1994.

Fetzer, E. J., and J. C. Gille, Gravity wave variance in

LIMS temperature, part I, Variability and comparison with background winds, *J. Atmos. Sci.*, *51*, 2461–2483, 1994.

Fritts, D. C., and G. D. Nastrom, Sources of mesoscale variability of gravity waves, part II, Frontal, convective, and jet stream excitation, *J. Atmos. Sci.*, *49*, 111–127, 1992.

Fritts, D. C., and T. E. VanZandt, Effects of Doppler shifting on the frequency spectra of atmospheric gravity waves, *J. Geophys. Res.*, *92*, 9723-9732, 1987.

Fritts, D. C., and T. E. VanZandt, Spectral estimates of gravity wave energy and momentum fluxes, part I, Energy dissipation, acceleration, and constraints, *J. Atmos. Sci.*, *50*, 3685-3694, 1993.

Fritts, D. C., T. Tsuda, T. E. VanZandt, S. A. Smith, T. Sato, S. Fukao, and S. Kato, Studies of velocity fluctuations in the lower atmosphere using the MU radar, part II, Momentum flux and energy densities, *J. Atmos. Sci.*, *47*, 51–66, 1990.

Hamilton, K., Climatological statistics of stratospheric inertia-gravity waves deduced from historical rocketsonde wind and temperature data, *J. Geophys. Res.*, *96*, 20,831–20,839, 1991.

Hirota, I., Climatology of gravity waves in the middle atmosphere, *J. Atmos. Sol. Terr. Phys.*, *46*, 767–773, 1984.

Hirota, I., and T. Niki, A statistical study of inertia-gravity waves in the middle atmosphere, *J. Meteorol. Soc. Jpn.*, *63*, 1055-1066, 1985.

Melbourne, W. G., et al., The application of spaceborne GPS to atmospheric limb sounding and global change monitoring, *JPL Publ.* 94-18, 1994.

Murayama, Y., T. Tsuda, S. Kato, and S. Fukao, Seasonal variation of gravity wave activity in the lower stratosphere observed with the MU radar, *J. Geophys. Res.*, *99*, 23,057–23,069, 1994.

Nastrom, G. D., and D. C. Fritts, Sources of mesoscale variability of gravity waves, part I, Topographic excitation, *J. Atmos. Sci.*, *49*, 101–110, 1992.

Nastrom, G. D., A. R. Hansen, T. Tsuda, M. Nishida, and R. Ware, A comparison of gravity wave energy observed by VHF radar and GPS/MET over central North America, *J. Geophys. Res.*, in press, 1999.

Pfister, L., W. Starr, R. Vraig, and M. Lowenstein, Small-scale motions observed by aircraft in the tropical lower stratosphere: Evidence for mixing and its relationship to large-scale flows, *J. Atmos. Sci.*, *43*, 3210–3225, 1986.

Pfister, L., K. R. Chan, T. B. Bui, S. Bowen, M. Legg, B. Gary, K. Kelly, M. Proffitt, and W. Starr, Gravity waves generated by a tropical cyclone during the STEP tropical field program, *J. Geophys. Res.*, *98*, 8611–8638, 1993.

Preusse, P., B. Schaeler, J. Bacmeister, and D. Offermann, Evidence for gravity waves in CRISTA temperatures, *Adv. Space Res.*, in press, 1998.

Rocken, C., et al., Analysis and validation of GPS/MET data in the neutral atmosphere, *J. Geophys. Res.*, *102*, 29,849–29,866, 1997.

Sato, K., Vertical wind disturbances in the troposphere and lower stratosphere observed by the MU radar, *J. Atmos. Sci.*, *47*, 2803–2817, 1990.

Shimizu, A., and T. Tsuda, Characteristics of Kelvin waves and gravity waves observed with radiosondes over Indonesia, *J. Geophys. Res.*, *102*, 26,159–26,171, 1997.

Smith, S. A., D. C. Fritts, and T. E. VanZandt, Evidence of a saturation spectrum of atmospheric waves, *J. Atmos. Sci.*, *44*, 1404-1410, 1987.

Tsuda, T., T. E. VanZandt, M. Mizumoto, S. Kato, and S. Fukao, Spectral analysis of temperature and Brunt-Väisälä frequency fluctuations observed by radiosondes, *J. Geophys. Res.*, *96*, 17,265-17,278, 1991.

Tsuda, T., Y. Murayama, K.-I. Oyama, H. Kanzawa, T. Nakamura, M. D. Yamanaka, S. Fukao, and S. Kato, Rocketsonde observations of the middle atmosphere dynamics at Uchinoura (31°N, 131°E) during DYANA campaign, part II, Characteristics of gravity waves, *J. Geomagn. Geoelectr.*, *44*, 1009–1023, 1992.

Tsuda, T., Y. Murayama, T. Nakamura, R. A. Vincent, A. H. Manson, C. E. Meek, and R. L. Wilson, Variations of the gravity wave characteristics with height, season and latitude revealed by comparative observations, *J. Atmos. Sol. Terr. Phys.*, *56*, 555–568, 1994.

VanZandt, T. E., A universal spectrum of buoyancy waves in the atmosphere, *Geophys. Res. Lett.*, *9*, 575-578, 1982.

VanZandt, T. E., A model for gravity wave spectra observed by Doppler sounding system, *Radio Sci.*, *20*, 1323-1330, 1985.

Ware, R., et al., GPS sounding of the atmosphere from low Earth orbit: Preliminary results, *Bull. Am. Meteorol. Soc.*, *77*, 19-40, 1996.

Wu, D. L., and J. W. Waters,Gravity-wave-scale temperature fluctuations seen by UARS MLS, *Geophys. Res. Lett.*, *23*, 3289–3292, 1996a.

Wu, D. L., and J. W. Waters, Satellite observations of atmospheric variances: A possible indication of gravity waves, *Geophys. Res. Lett.*, *23*, 3631–3634, 1996b.

M. Nishida and T. Tsuda, Kyoto Univ., Uji, Kyoto 611-0011, Japan.(tsuda@kurasc.kyoto-u.ac.jp)

C. Rocken and R. H. Ware, GPS/MET Project, GPS Science and Technology (GST) Program, University Corporation for Atmospheric Research (UCAR), Boulder, CO 80307-3000.

(Received February 5, 1999; revised September 7, 1999; accepted September 15, 1999.)